

Article

Polarization-Insensitive, Wideband Terahertz Absorber Comprised of Fan-like Metasurface

Meshari Alsharari ¹, Khaled Aliqab ^{1,*}, Ammar Armghan ^{1,*}, Muhammad Saqlain ²
and Muhammad Abuzar Baqir ²

¹ Department of Electrical Engineering, College of Engineering, Jouf University, Sakaka 72388, Saudi Arabia; mmaalsharari@ju.edu.sa

² Department of Electrical and Computer Engineering, COMSATS University Islamabad, Islamabad 45550, Pakistan; saqlain@cuisahiwal.edu.pk (M.S.); abuzar@cuisahiwal.edu.pk (M.A.B.)

* Correspondence: kmaliqab@ju.edu.sa (K.A.); aarmghan@ju.edu.sa (A.A.)

Abstract: In this manuscript, we studied a wideband metasurface-based terahertz (THz) absorber. The metasurface of the proposed absorber was comprised of fan-like periodic resonators made of nickel (Ni). The absorptivity of the proposed absorber was analyzed from 3.5 to 5 THz. The wideband absorptivity is observed with an absorption above 75% from 3.7 to 4.7 THz. The polarization-insensitive behavior of the absorber is depicted due to the symmetric nature of the top metasurface. The absorption feature was also analyzed for the transverse electric (TE) and transverse magnetic (TM) operating modes for the obliquity of the incidence wave. The surface current density shows that absorption is achieved due to the electric resonance of the proposed absorber. The proposed absorber would be useful for several applied areas covering medical science, communication, safety supervision, chemical sensing, and imaging.

Keywords: metasurface; terahertz; wideband absorber



Citation: Alsharari, M.; Aliqab, K.; Armghan, A.; Saqlain, M.; Baqir, M.A. Polarization-Insensitive, Wideband Terahertz Absorber Comprised of Fan-like Metasurface. *Symmetry* **2023**, *15*, 1258. <https://doi.org/10.3390/sym15061258>

Academic Editor: Vasilis K. Oikonomou

Received: 6 May 2023

Revised: 2 June 2023

Accepted: 6 June 2023

Published: 14 June 2023



Copyright: © 2023 by the authors. Licensee MDPI, Basel, Switzerland. This article is an open access article distributed under the terms and conditions of the Creative Commons Attribution (CC BY) license (<https://creativecommons.org/licenses/by/4.0/>).

1. Introduction

Over the years, the terahertz (THz) wave has been in the spectrum range of 0.1–10 THz and has shown great potential for several promising applications: THz imaging for medicine and security, non-destructive testing by THz cameras, and ultra-high data rates for wireless communication [1–5]. Among several features, absorption is one of the distinctive characteristics of the THz wave when interacting with artificial structures, and therefore it shows its suitability for metamaterial-based devices [6–9]. For instance, several reported studies related to THz metamaterial-based absorbers have been presented [10–19]. For instance, a few studies [10–13] include a simple metal structure and show significant absorption within the THz band. Besides this, metamaterial-based absorbers operating in the THz band can be designed for narrowband and wideband operations to support several promising applications, such as filtering, biological imaging, stealth technology, and communication.

To achieve wideband operation in the THz operating region, several multilayer metamaterial structures have been demonstrated that show high absorption peaks due to different structures [20–30]. These multilayer metamaterial-based absorbers have complex designs and a difficult fabrication process, leading them to show complications in integrating with commercial technologies and therefore ultimately increasing the cost. Several works on multilayer-based wideband absorbers have been reported based on theoretical studies [20–23] and experimental demonstrations [24,25]. On the other hand, the single-layer structure shows several benefits compared to multilayer-based wideband absorbers, including a simple fabrication process and low cost. One simple method of attaining such a design is using multiple resonating structures with different-sized unit cells and causing a high absorption over the wide portion of the THz spectrum [31,32].

For instance, a single-layer structure of a unit cell comprising three resonators with an I-shaped geometry has been designed to attain a significantly high absorptivity within the THz band range of 0.899–0.939 THz [33]. Moreover, the selection of metal is vital when considering the design of metamaterial devices. Within this context, noble metals, such as nickel, gold, and tungsten, have been widely used for the construction of metamaterial absorbers [34–36]. These metals can operate in different frequency bands and effectively perform under high-temperature environments. Among these, nickel (Ni) is considered low-cost and can absorb the THz wave energy over a wide spectrum range; hence, further investigations on THz metasurface-based absorption devices is required when considering the wideband operational ability, simple structure, and easy fabrication process. As a result, nickel-based THz absorbers can be useful in numerous practical areas: imaging in medical and security sectors, communication, etc.

In this study, we aim to investigate the operation of a wideband nickel-based THz absorber with a fan-like structure operating within 3.5–5 THz. The structure of the absorber comprises a top layer of nickel having a fan-like shape and 2 μm followed by a silicon dioxide (SiO_2) layer to facilitate THz wave penetration; furthermore, the ground layer is made of silver (Ag), with a thickness of 1 μm , and provides a perfect reflection to the striking THz waves. The proposed THz absorber has shown more than 75% absorption over the frequency band ranging from 3.7–4.7 THz. Further, the absorber shows a polarization-independent nature due to the symmetrical geometry of the top metasurface. We have also investigated the absorption process for the obliquity of the incident THz wave when considering both transverse electric and magnetic operating modes. Furthermore, we have conducted some analyses on the surface current distribution, and the results reveal that absorption is achieved due to electric resonance. This metasurface-based absorber can be useful in several exciting fields: THz imaging, sensing, and communication.

2. Materials and Methods

Our proposed metasurface-based THz absorber comprises a unit cell consisting of a top metasurface layer and a metal-made bottom layer that is separated from the top layer by a dielectric material layer, and this configuration can be seen in Figure 1. Part (a) and part (b) of Figure 1 represent the 2D and 3D images of the proposed fan-like unit cell and its panel. From Figure 1a, we can see the geometric values of the proposed unit cell, where the period is taken as $P = 100 \mu\text{m}$. Here, we are taking the same size for all arms of the top metasurface in terms of arm length and width, the other dimensions are $w = 10 \mu\text{m}$ and $l = 20 \mu\text{m}$, and the circular disk radius r is 2 μm . The thickness of the dielectric layer is 10 μm to allow maximum penetration of THz waves. The thickness of the bottom layer made of silver is 1 μm to prevent any incidence of THz wave transmission. Besides these, the dielectric constant of SiO_2 is kept at 2.25, and the dielectric constant of Ni is deduced by using the Johnson and Christy model [37].

We have used CST studio software for this simulation of a unit cell. For this, unit cell boundary conditions are applied along the x- and y-axes, and open boundary conditions are applied in the z-direction, respectively. A plane wave propagating along the z-axis is excited on the top surface of the absorber. The relationship of absorption, transmission, and reflection can be found by using S-parameters [38]:

$$A = 1 - |S_{11}|^2 - |S_{21}|^2. \quad (1)$$

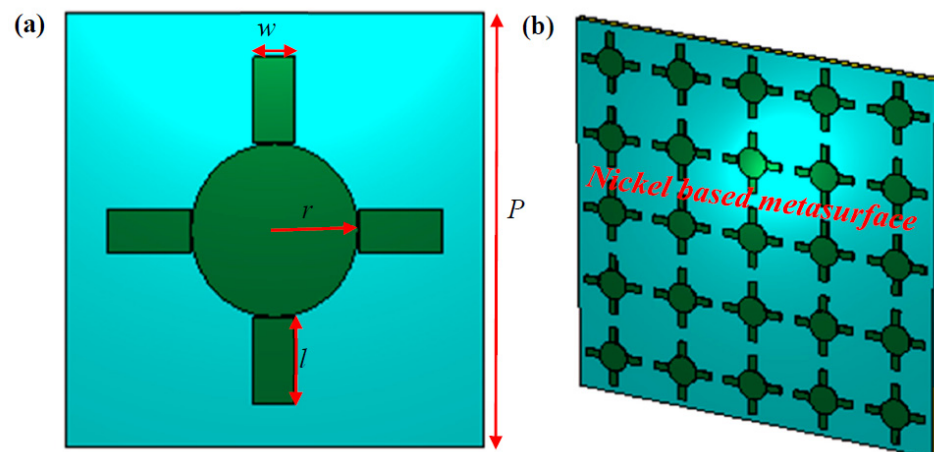


Figure 1. Schematic demonstration of the metasurface-based absorber: (a) unit cell with 2D front view; (b) metasurface-based panel with 3D view.

The parameter S_{11} represents the reflection coefficient, and S_{21} is the transmission coefficient.

We simplify Equation (1) while only considering the S_{11} parameter term due to the perfect reflection of the bottom layer made of silver with a 1 μm thickness. Therefore, the above equation can be further simplified as:

$$A = 1 - |S_{11}|^2. \quad (2)$$

Now, we can directly calculate the absorption of the proposed metasurface-based THz absorber using Equation (2).

3. Results

Here, we present the absorption characteristics while considering the operating THz frequency band using S-parameters. The different stages of the metasurface-based THz absorber and their corresponding absorption results are visualized in Figure 2. Moreover, the optimized results of the absorption over the operating THz band are obtained by changing the structure and parametric values and are demonstrated in the part (d) of Figure 2. Now, we begin our discussion while considering stage one of the proposed absorber, where a circular disk with a radius of 2 μm is taken as a metasurface, and this arrangement can be seen in Figure 2a. In this case, an absorption of more than 75% is noticed from 3.7–4.7 THz. After that, the absorption value starts decreasing with a further increase in the frequency, and this decreasing trend shows the existence of a weak Localized Surface Plasmon Resonance (LSPR). It is important to note that a weak LSPR, referred to as LSPR mode, causes a weak interaction between the incident wave and plasmon structure [39]. However, the same absorption over the considered frequency band is noted under the influence of TE and TM operating modes. Meanwhile, the structure of stage two and stage three of the proposed design is extended while adding an arm-like shape on both sides of the circular disk in the horizontal and vertical directions, and their dimensions are set as $20 \times 10 \mu\text{m}^2$ and are shown in Figure 2b,c. From their corresponding plots, we can notice the same absorption trend for both TE and TM modes over the entire frequency band. Meanwhile, Figure 2d shows the absorption plots for the optimum design and is named stage four. Here, the metasurface design is composed of a fan-like structure, and its parametric values are considered the same as those discussed in the above section. From the corresponding plot, we can notice that a high absorption value of more than 75% is obtained over the frequency band ranging from 3.7–4.7 THz. This high absorption is due to the strong LSPR effect created by the proposed optimized structure. Moreover, we can observe that the absorption value remains the same under the influence of both TE and TM operating modes and is evident in the symmetrical geometry of the proposed metasurface structure.

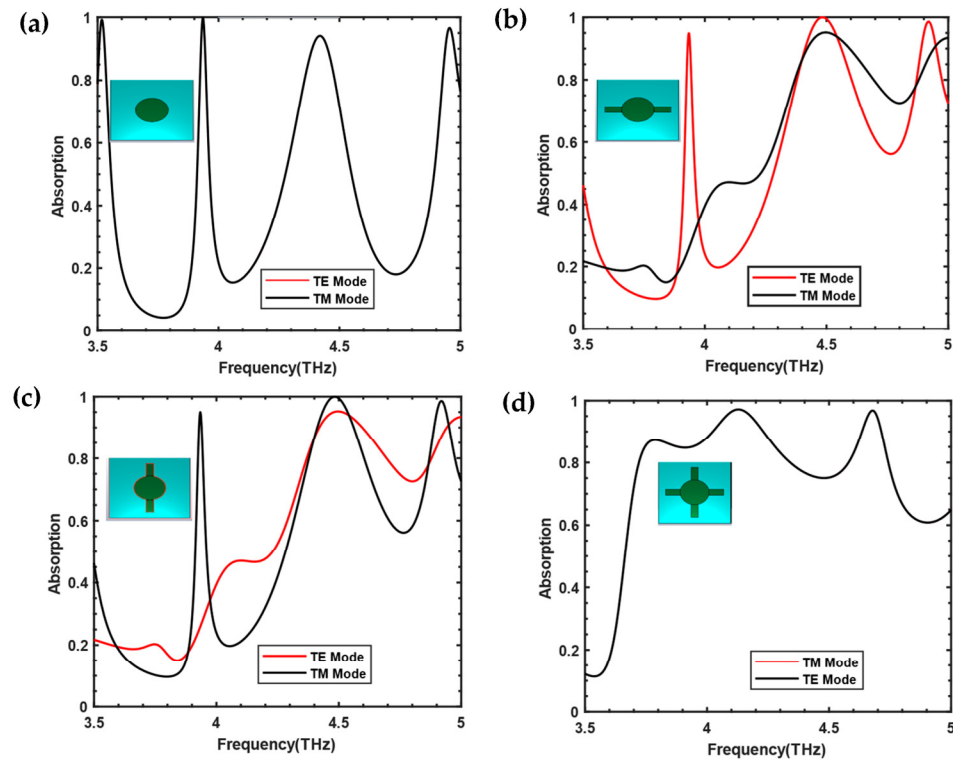


Figure 2. Absorption results when considering the incident THz wave for different metasurface-based structures: (a) stage one, (b) stage two, (c) stage three, and (d) stage four.

Next, we discuss the analysis of the absorption of the proposed metasurface-based THz absorber in relation to several extracted parameters, such as the impedance, refractive index, permeability, and permittivity in terms of S-parameters [38]. It is important to note that the analysis of these extracted parameters will further help readers to easily understand the absorption mechanism of the proposed absorber. The relation of the impedance Z with S-parameters can be expressed as:

$$Z = \sqrt{\frac{(1 + S_{11})^2 - S_{21}^2}{(1 - S_{11})^2 - S_{21}^2}} \quad (3)$$

where $Z = Re(Z) + Im(Z)$, and the absorption coefficient in terms of the impedance is represented as [38]:

$$\alpha = \frac{4Re(Z)}{[1 + Re(Z)]^2 + [Im(Z)]^2} \quad (4)$$

Similarly, we can relate the thickness of the absorber d with the medium refractive index n , represented as:

$$n = \frac{iln(e^{ik_0d})}{k_0d} \quad (5)$$

where k_0 represents the wavenumber. Moreover, for a better understanding, we can relate the relationship of the refractive index with S-parameters, and for this, $e^{ink_0d} = Y \pm i\sqrt{1 - Y^2}$, where $Y = 1/2S_{21}(1 - S_{11}^2 + S_{21}^2)$. Now, we can write the mathematical relation of the permittivity (ϵ_{eff}) and permeability (μ_{eff}) in terms of the impedance and refractive index as $\epsilon_{eff} = \frac{n}{Z}$ and $\mu_{eff} = n \times Z$.

From Equation (4), we can derive that a perfect absorption is achieved when the following condition is met, i.e., ($Z = Z_m/Z_o = 1$), where Z , Z_m and Z_o denote the normalized impedance, material impedance and free space characteristic impedance, respectively. For a perfect absorption, the real part of the impedance approaches unity. Furthermore, the

matching of the impedance of the proposed absorber with the free-space impedance is a result of the LSPR effect. In Figure 3a, we can see both the real parts of the impedance and the refractive index profile over the operating frequency range of 3.5–5 THz. It can be noticed that the normalized impedance varies over the entire frequency range. Furthermore, a normalized impedance with a near-unity value can be noticed over the frequency span of 4–5 THz, where high absorption peaks exist (visualized in part (d) of Figure 2). Besides that, the symmetrical structure of the proposed absorber causes the impedance to remain the same for both operating modes. Similarly, the refractive index profile remains negative over the large portion of the spectrum, and this profile is clearly visualized in the inset of Figure 3a. The frequency-dependent permittivity and permeability profiles are shown in parts (b) and (c) of Figure 3. From the corresponding plots, one can clearly see that both the permittivity and permeability show a decreasing trend over most parts of the operating frequency region, as noted in Figure 3b. Meanwhile, the imaginary part of the permittivity decreases up to 4.1 THz. After that, this value shows increasing and decreasing trends above this frequency band, as noticed in part (c) of Figure 3.

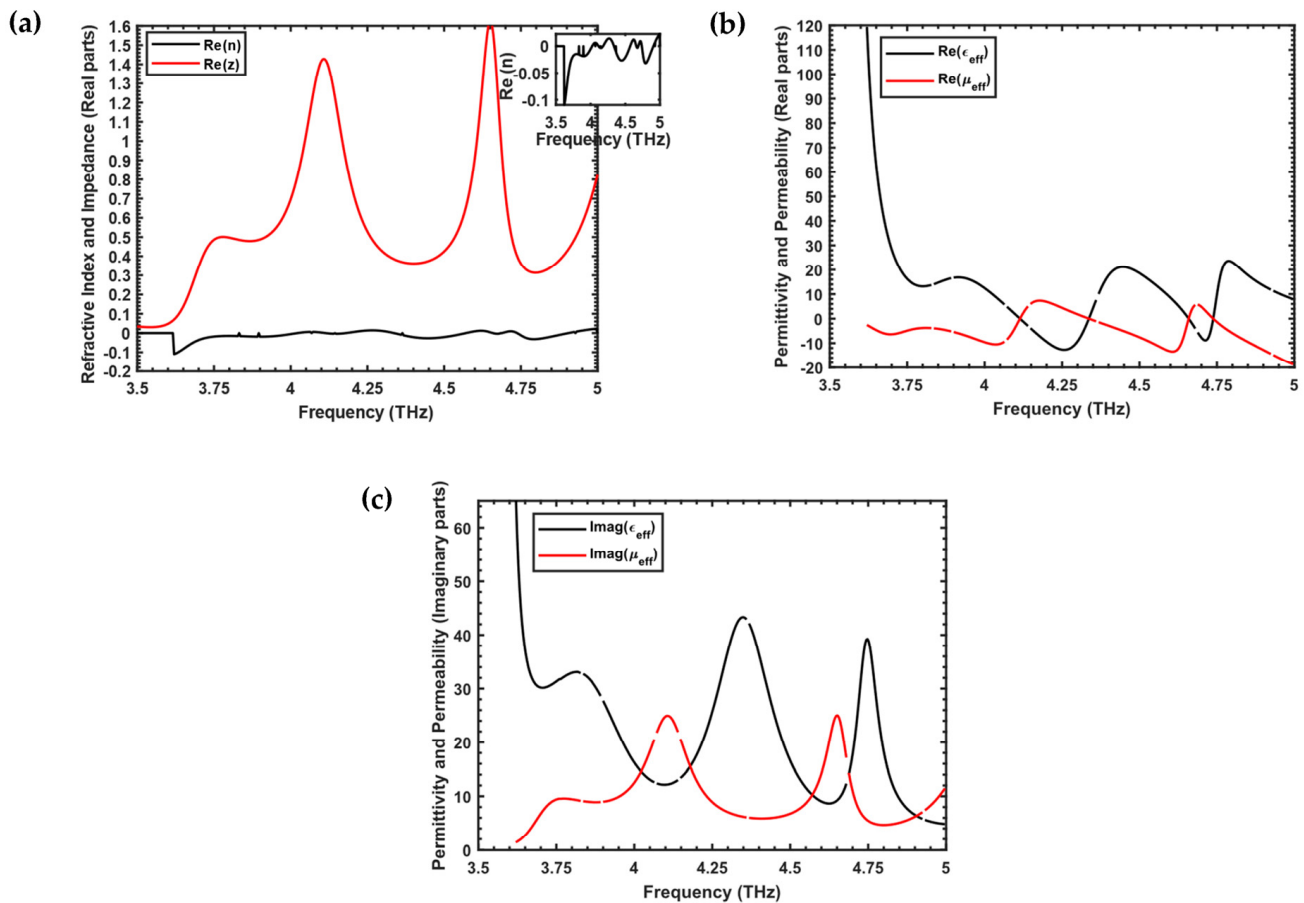


Figure 3. Retrieved parameters of the proposed metamaterial absorber. (a) Impedance and refractive index profile; (b) permittivity and permeability (real parts); (c) permittivity and permeability (imaginary parts).

Now, we analyze the angle-dependent absorption of the metasurface-based THz absorber, and Figure 4 shows the simulation results. The analysis work for this section has been considered for the angle range from $\theta = 0^\circ$ to 60° with a step size of 20° , and both operating modes (TE and TM) are considered. From the corresponding TE mode plot (Figure 4a), the absorption remains an average of more than 75% for $\theta = 0^\circ$ over the operating frequency range of 3.7–4.7 THz. Similarly, for $\theta = 20^\circ$ and considering the TE mode, the overall absorption decreases to an average value of slightly more than 65%. For

the higher angles ($\theta = 40^\circ$ and 60°), the absorption further decreases and shows a weak LSPR effect for a higher obliquity of incidence. Therefore, the proposed THz absorber shows sensitivity to the higher angular variation. On the other hand, Figure 4b shows the absorption curves versus angular variation for the TM mode. One can see from the corresponding plot that the overall absorption is high for this mode of operation when compared to the TE mode. Furthermore, a few portions of the operating range show a relatively low absorption due to the weak LSPR effect. It is worth noting that angular stability can be attained by carefully optimizing the unit cell of the metamaterial absorber. For this, a few state-of-the-art studies have shown angular stability while developing symmetric unit cells of metamaterial-based absorbers [40,41].

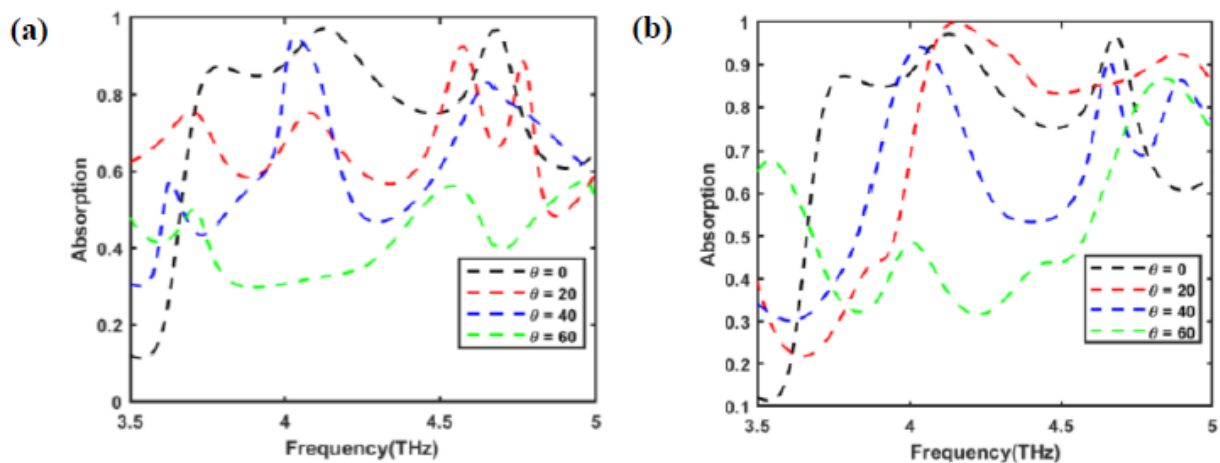


Figure 4. Absorption over the wide incidence angle range of 0° to 60° when considering both operating modes: (a) TE-mode and (b) TM-mode.

Next, the impact of polarization on the absorption characteristics of the incident THz wave is analyzed, and Figure 5 shows the results. From the corresponding plot, one can see that the proposed absorber shows a polarization-independent nature. This property of the proposed absorber is achieved due to the fourfold symmetrical structure. Moreover, for this symmetric arrangement, LSPR remains the same when a change in the polarization state of the incident THz wave is considered, as shown in Figure 5. We can conclude that the absorption characteristics are not dependent on the variation in the polarization state. This feature of the proposed absorber can make it useful in several practical applications, such as THz imaging and sensing, etc. It has been reported that polarization-insensitive metamaterial-based absorbers are useful for imaging and sensing applications [42,43]. The polarization-independent sensing system and detector provides reliable results, regardless of the polarization state of the incoming light.

Furthermore, we explain the absorption of the proposed metasurface-based THz absorber in more detail when considering the distribution of the surface current density at different operating THz frequencies. For this, we consider two operating frequencies, 4.124 and 4.68 THz, respectively; their corresponding surface current densities' plots are shown in Figure 6. The surface current density plots of the top metasurface and reflecting ground layers are taken at $f = 4.124$ THz and shown in parts (a,b) of Figure 6. From these plots, we can see that the surface current density is maximally confined on a fan-like metallic resonator. Further, the vectors of the surface current densities of the top metasurface and reflecting bottom layer are parallel, which evokes the electric resonance. Therefore, the LSPR is attained due to electric resonance, which in turn produces absorption. Similarly, Figure 6c,d show the surface current densities for the top and bottom layers at 4.68 THz. From these plots, we can find a similar observation as for 4.124 THz.

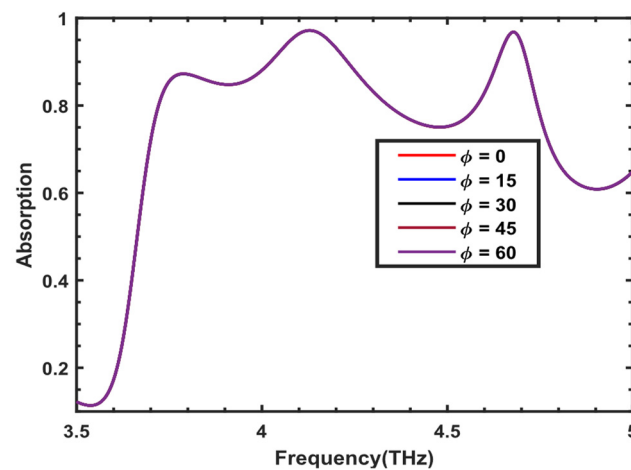


Figure 5. The relationship between absorption and varying polarizations of the incident THz wave over a wide angular range, considering both TE and TM operating modes.

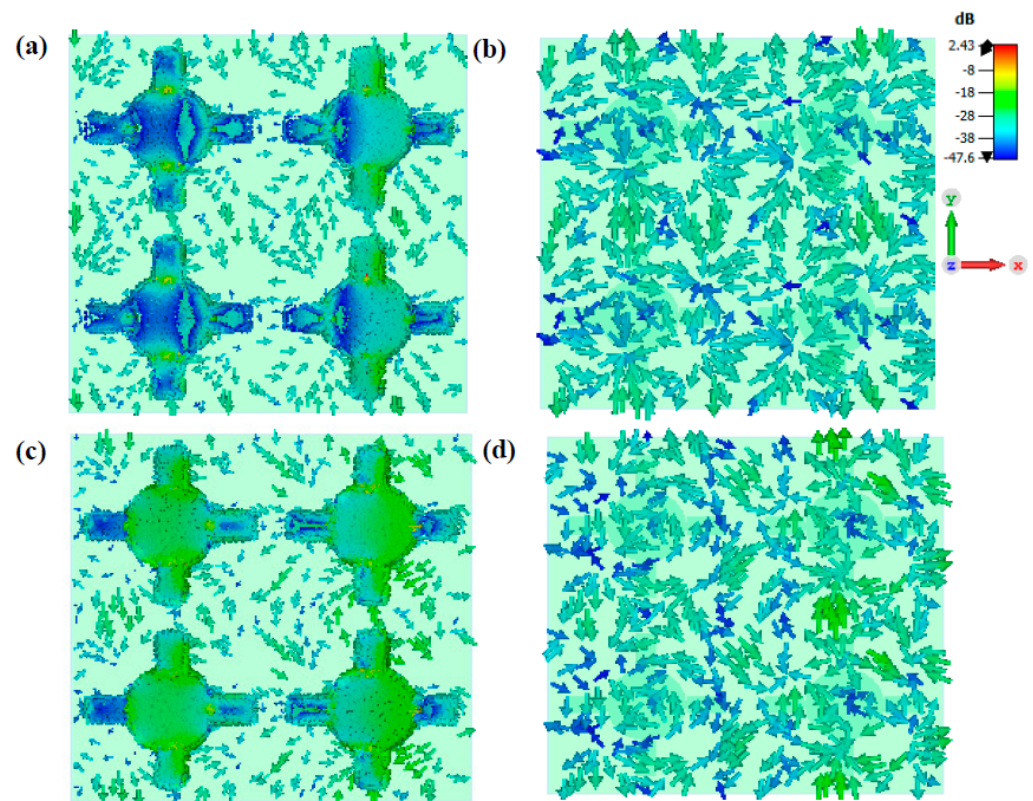


Figure 6. Surface current density of the proposed fan-like metasurface absorber. (a) Top metasurface for $f = 4.124$ THz; (b) bottom layer for $f = 4.124$ THz; (c) top metasurface for $f = 4.68$ THz; (d) bottom layer for $f = 4.68$ THz.

Finally, the performance of the proposed metasurface-based THz absorber is compared with several state-of-the-art works in terms of some important parameters, as shown in Table 1. Moreover, Table 1 shows the absorption performances of recently reported works containing different geometrical structures. Our proposed THz absorber shows a better performance in terms of absorption over the wideband of the operating spectrum, has a simple design consisting of a single-layer structure, and uses cost-effective Ni material for the top metasurface. We can notice from Table 1 that the authors in reference [44] show a broadband THz absorber made of a biaxial hyperbolic structure, and high absorption

characteristics can be achieved when employing a large number of layers on the bottom surface, which makes this structure more complex when compared with our proposed work.

Table 1. Performance of proposed THz absorber compared with state-of-the-art works.

Geometry	Comment	Bandwidth Absorption > 75%	Layers
Present Work Fan-like shaped	Wideband operation and low-cost	3.7–4.7 THz (1 THz)	1
Square rings [24]	Wideband and expensive	0.79–1.4 THz (0.61 THz)	3
Stacked shaped [22]	Wideband and expensive	1.68–2.25 THz (0.57 THz)	3
Square-rings [45]	Single layer and expensive	0.6–1.25 THz (0.65 THz)	1
Biaxial hyperbolic [44]	Wideband and Multi layers	3–10 THz (7 THz)	20

4. Conclusions

In the previous discussion, a fan-like metasurface-based wideband THz absorber is analyzed. The extraction parameters, such as the impedance, refractive index, permittivity, and permeability, are investigated to study the material properties of the proposed metasurface-based absorber. Further, the surface current densities are considered for different absorption peaks of the absorber, showing that the absorption is achieved due to the electric resonance. Moreover, it is observed that the proposed absorber shows a polarization-independent nature to the incident THz wave as a result of the fourfold symmetrical structure of the unit cell of the metasurface. The proposed absorber can be useful for several exciting fields, including communication and THz for imaging and sensing.

Author Contributions: Conceptualization, M.A., A.A. and M.A.B.; Data curation, M.A. and M.A.B.; Formal analysis, M.A., A.A. and M.S.; Investigation, M.A. and K.A.; Methodology, M.A., K.A., M.S. and M.A.B.; Project administration, M.A.B.; Resources, K.A. and A.A.; Software, M.A. and M.S.; Supervision, K.A., A.A. and M.A.B.; Validation, K.A., M.S. and M.A.B.; Visualization, M.A. and M.S.; Writing—original draft, M.A., A.A., M.S. and M.A.B.; Writing—review and editing, K.A. and M.S. All authors have read and agreed to the published version of the manuscript.

Funding: The authors extend their appreciation to the Deputyship for Research & Innovation, Ministry of Education in Saudi Arabia for funding this research work through the project number 223202.

Data Availability Statement: Not applicable.

Conflicts of Interest: The authors declare no conflict of interest.

References

1. Yao, G.; Ling, F.; Yue, J.; Luo, C.; Ji, J.; Yao, J. Dual-band tunable perfect metamaterial absorber in the THz range. *Opt. Express* **2016**, *24*, 1518–1527. [[CrossRef](#)] [[PubMed](#)]
2. Chen, H.; Chen, T.-H.; Tseng, T.-F.; Lu, J.-T.; Kuo, C.-C.; Fu, S.-C.; Lee, W.-J.; Tsai, Y.-F.; Huang, Y.-Y.; Chuang, E.Y.; et al. High-sensitivity in vivo THz transmission imaging of early human breast cancer in a subcutaneous xenograft mouse model. *Opt. Express* **2011**, *19*, 21552–21562. [[CrossRef](#)] [[PubMed](#)]
3. Shen, Y.C.; Lo, T.; Taday, P.F.; Cole, B.E.; Tribe, W.R.; Kemp, M.C. Detection and identification of explosives using terahertz pulsed spectroscopic imaging. *Appl. Phys. Lett.* **2005**, *86*, 377. [[CrossRef](#)]
4. Yoshida, H.; Ogawa, Y.; Kawai, Y.; Hayashi, S.; Hayashi, A.; Otani, C.; Kato, E.; Miyamaru, F.; Kawase, K. Terahertz sensing method for protein detection using a thin metallic mesh. *Appl. Phys. Lett.* **2007**, *91*, 97. [[CrossRef](#)]
5. Wang, S.; Lu, Z.; Li, W.; Jia, S.; Zhang, L.; Qiao, M.; Pang, X.; Idrees, N.; Saqlain, M.; Gao, X.; et al. 26.8-m THz wireless transmission of probabilistic shaping 16-QAM-OFDM signals. *APL Photon.* **2020**, *1*, 056105. [[CrossRef](#)]
6. Cong, L.; Tan, S.; Yahiaoui, R.; Yan, F.; Zhang, W.; Singh, R. Experimental demonstration of ultrasensitive sensing with terahertz metamaterial absorbers: A comparison with the metasurfaces. *Appl. Phys. Lett.* **2015**, *106*, 031107. [[CrossRef](#)]
7. Li, F.; Jiang, X.; Zhao, J.; Zhang, S. Graphene oxide: A promising nanomaterial for energy and environmental applications. *Nano Energy* **2015**, *82*, 229–237. [[CrossRef](#)]
8. He, X.; Gao, P.; Shi, W. A further comparison of graphene and thin metal layers for plasmonics. *Nanoscale* **2016**, *8*, 10388–10397. [[CrossRef](#)]

9. Lin, F.; Shi, W.; He, X.; Zhong, X. Investigation of graphene assisted tunable terahertz metamaterials absorber. *Opt. Mater. Express* **2016**, *6*, 331.
10. Wang, B.X.; Zhai, X.; Wang, G.Z.; Huang, W.Q.; Wang, L.L. Quad-Band Terahertz Absorber Based on a Simple Design of Metamaterial Resonator. *IEEE Photon. J.* **2015**, *8*, 5502408. [[CrossRef](#)]
11. Wang, B.-X.; Wang, L.-L.; Wang, G.-Z.; Huang, W.-Q.; Li, X.-F.; Zhai, X. A broadband, polarisation-insensitive and wide-angle coplanar terahertz metamaterial absorber. *Eur. Phys. J. B* **2014**, *87*, 98. [[CrossRef](#)]
12. Wang, B.-X.; Wang, L.-L.; Wang, G.-Z.; Huang, W.-Q.; Li, X.-F.; Zhai, X. Metamaterial-Based Low-Conductivity Alloy Perfect Absorber. *J. Light. Technol.* **2014**, *32*, 2293–2298. [[CrossRef](#)]
13. Ma, Y.; Chen, Q.; Grant, J.; Saha, S.C.; Khalid, A.; Cumming, D.R.S. A terahertz polarization insensitive dual band metamaterial absorber. *Opt. Lett.* **2011**, *36*, 945–947. [[CrossRef](#)] [[PubMed](#)]
14. Fan, Y.; Yang, R.; Li, Z.; Zhao, Y.; Tian, J.; Zhang, W. Narrowband metamaterial absorbers based on interlaced T-shaped all-dielectric resonators for sensing application. *J. Opt. Soc. Am. B* **2022**, *39*, 2863. [[CrossRef](#)]
15. Feng, G.; Chen, Z.; Wang, X.; Liu, X.; Sun, F.; Yang, Y. Ultra-broadband terahertz absorber based on double truncated pyra-mid structure. *Mater. Today Commun.* **2022**, *31*, 103624. [[CrossRef](#)]
16. Zhao, J.; Cheng, Y. Temperature-Tunable Terahertz Perfect Absorber Based on All-Dielectric Strontium Titanate (STO) Resonator Structure. *Adv. Theory Simul.* **2022**, *5*, 2200520. [[CrossRef](#)]
17. Song, Z.; Chen, A.; Zhang, J. Terahertz switching between broadband absorption and narrowband absorption. *Opt. Express* **2022**, *28*, 2037–2044. [[CrossRef](#)]
18. Weng, X.; Wang, J.; Xu, C.; Wang, Y.; Liao, Y.; Wang, X. Dual-Band Perfect Absorber Based on All-Dielectric GaAs Metasurface for Terahertz Wave. *Plasmonics* **2023**, *18*, 521–528. [[CrossRef](#)]
19. Cheng, Y.; Qian, Y.; Luo, H.; Chen, F.; Cheng, Z. Terahertz narrowband perfect metasurface absorber based on micro-ring-shaped GaAs array for enhanced refractive index sensing. *Phys. E Low-Dimens. Syst. Nanostruct.* **2023**, *146*, 115527. [[CrossRef](#)]
20. Pan, W.; Yu, X.; Zhang, J.; Zeng, W. A Novel Design of Broadband Terahertz Metamaterial Absorber Based on Nested Circle Rings. *IEEE Photon. Technol. Lett.* **2016**, *28*, 2335. [[CrossRef](#)]
21. He, X.-J.; Yan, S.-T.; Ma, Q.-X.; Zhang, Q.-F.; Jia, P.; Wu, F.-M.; Jiang, J.-X. Broadband and polarization-insensitive terahertz absorber based on multilayer metamaterials. *Opt. Commun.* **2015**, *340*, 44–49. [[CrossRef](#)]
22. He, S.; Jin, Y.; Ye, Y.Q. Omnidirectional, polarization-insensitive and broadband thin absorber in the terahertz regime. *J. Opt. Soc. Am. B* **2010**, *27*, 498. [[CrossRef](#)]
23. Liu, S.; Chen, H.; Cui, T.J. A broadband terahertz absorber using multi-layer stacked bars. *Appl. Phys. Lett.* **2015**, *106*, 163702. [[CrossRef](#)]
24. Zhu, J.F.; Ma, Z.F.; Sun, W.J.; Ding, F.; He, Q.; Zhou, L.; Ma, Y.G. Ultra-broadband terahertz metamaterial absorber. *Appl. Phys. Lett.* **2014**, *105*, 4773. [[CrossRef](#)]
25. Liu, Y.; Qian, Y.; Hu, F.; Jiang, M.; Zhang, L. A dynamically adjustable broadband terahertz absorber based on a vanadium dioxide hybrid metamaterial. *Results Phys.* **2020**, *19*, 103384. [[CrossRef](#)]
26. Banerjee, S.; Dutta, P.; Basu, S.; Mishra, S.K.; Appasani, B.; Nanda, S.; Abdulkarim, Y.I.; Muhammadsharif, F.F.; Dong, J.; Jha, A.V.; et al. A New Design of a Terahertz Metamaterial Absorber for Gas Sensing Applications. *Symmetry* **2022**, *15*, 24. [[CrossRef](#)]
27. Yan, D.; Li, X.; Ma, C.; Qiu, G.; Cao, M.; Li, J.; Guo, S. Terahertz Refractive Index Sensing Based on Gradient Metasurface Coupled Confined Spoof Surface Plasmon Polaritons Mode. *IEEE Sens. J.* **2021**, *22*, 324–329. [[CrossRef](#)]
28. Nickpay, M.-R.; Danaie, M.; Shahzadi, A. Highly Sensitive THz Refractive Index Sensor Based on Folded Split-Ring Metamaterial Graphene Resonators. *Plasmonics* **2021**, *17*, 237–248. [[CrossRef](#)]
29. Banerjee, S.; Dutta, P.; Jha AK, V.; Tripathi, P.R.; Srinivasulu, A.; Appasani, B.; Ravariu, C. A triple band highly sensitive refractive index sensor using terahertz metamaterial perfect absorber. *Prog. Electromagn. Res. M* **2022**, *107*, 13–23. [[CrossRef](#)]
30. Cheng, Y.; Nie, Y.; Gong, R. Analysis of single-layer metamaterial absorber with reflection theory. *Opt. Laser Technol.* **2013**, *48*, 415. [[CrossRef](#)]
31. Wang, G.D.; Liu, M.H.; Hu, X.W.; Kong, L.H.; Cheng, L.L.; Chen, Z.Q. Broadband and ultra-thin terahertz metamaterial absorber based on multi-circular patches. *Eur. Phys. J. B* **2013**, *86*, 1. [[CrossRef](#)]
32. Huang, L.; Chowdhury, D.R.; Ramani, S.; Reiten, M.T.; Luo, S.-N.; Taylor, A.J.; Chen, H.-T. Experimental demonstration of terahertz metamaterial absorbers with a broad and flat high absorption band. *Opt. Lett.* **2012**, *37*, 154–156. [[CrossRef](#)]
33. Rufangura, P.; Sabah, C. Design and characterization of a dual-band perfect metamaterial absorber for solar cell applications. *J. Alloys Compd.* **2016**, *671*, 43–50. [[CrossRef](#)]
34. Geldmeier, J.; König, T.; Mahmoud, M.A.; El-Sayed, M.A.; Tsukruk, V.V. Tailoring the Plasmonic Modes of a Grating-Nanocube Assembly to Achieve Broadband Absorption in the Visible Spectrum. *Adv. Funct. Mater.* **2014**, *24*, 6797. [[CrossRef](#)]
35. Cao, T.; Wei, W.C.; Simpson, R.E.; Zhang, L.; Cryan, M.J.; Han, S.; Lee, B.J. Broadband polarization-independent perfect absorber using a phase-change metamaterial at visible frequencies. *Sci. Rep.* **2014**, *4*, 3955. [[CrossRef](#)] [[PubMed](#)]
36. Han, S.; Lee, B.J. Electromagnetic resonance modes on a two-dimensional tandem grating and its application for broadband absorption in the visible spectrum. *Opt. Express* **2015**, *24*, A202. [[CrossRef](#)]
37. Johnson, P.B.; Christy, R.W. Optical Constants of the Noble Metals. *Phys. Rev. B* **1972**, *6*, 4370–4379. [[CrossRef](#)]
38. Smith, D.R.; Vier, D.C.; Koschny, T.; Soukoulis, C.M. Electromagnetic parameter retrieval from inhomogeneous metamaterials. *Phys. Rev. E* **2005**, *71*, 036617. [[CrossRef](#)]

39. Amiri, M.; Tofigh, F.; Shariati, N.; Lipman, J.; Abolhasan, M. Review on Metamaterial Perfect Absorbers and Their Applications to IoT. *IEEE Internet Things J.* **2020**, *8*, 4105–4131. [[CrossRef](#)]
40. Liang, Y.; Lin, H.; Lin, S.; Wu, J.; Li, W.; Meng, F.; Yang, Y.; Huang, X.; Jia, B.; Kivshar, Y. Hybrid anisotropic plasmonic metasurfaces with multiple resonances of focused light beams. *Nano Lett.* **2020**, *21*, 8917–8923. [[CrossRef](#)]
41. Ebrahimi, A.; Ako, R.T.; Lee, W.S.; Bhaskaran, M.; Sriram, S.; Withayachumnankul, W. High-Q Terahertz Absorber with Stable Angular Response. *IEEE Trans. Terahertz Sci. Technol.* **2020**, *10*, 204–211. [[CrossRef](#)]
42. Cai, Y.; Huang, Y.; Zhu, K.; Wu, H. Symmetric metasurface with dual band polarization-independent high-Q resonances governed by symmetry-protected BIC. *Opt. Lett.* **2021**, *46*, 4049–4052. [[CrossRef](#)] [[PubMed](#)]
43. Lin, D.; Holsteen, A.L.; Maguid, E.; Fan, P.; Kik, P.G.; Hasman, E.; Brongersma, M.L. Polarization-independent metasurface lens employing the Pancharatnam-Berry phase. *Opt. Express* **2018**, *26*, 24835–24842. [[CrossRef](#)] [[PubMed](#)]
44. Liu, J.; Chen, W.; Ma, W.-Z.; Chen, Y.-S.; Deng, X.-C.; Zhuang, P.-P.; Ye, Q. Biaxial hyperbolic metamaterial THz broadband absorber utilizing anisotropic two-dimensional materials. *Results Phys.* **2021**, *22*, 103818. [[CrossRef](#)]
45. Shen, G.; Zhang, M.; Ji, Y.; Huang, W.; Yu, H.; Shi, J. Broadband terahertz metamaterial absorber based on simple multi-ring structures. *AIP Adv.* **2018**, *8*, 075206. [[CrossRef](#)]

Disclaimer/Publisher’s Note: The statements, opinions and data contained in all publications are solely those of the individual author(s) and contributor(s) and not of MDPI and/or the editor(s). MDPI and/or the editor(s) disclaim responsibility for any injury to people or property resulting from any ideas, methods, instructions or products referred to in the content.